

Low-lying Dirac eigenmodes and monopoles in 4D compact QED

Toru T. Takahashi *

December 25, 2018

Abstract

We study the correlations between the fluctuations of low-lying Dirac eigenfunctions and monopoles in quenched compact QED at $\beta=0.99$, 1.01 and 1.03, employing $12^3 \times 12$ lattices and the overlap formalism for the fermion action. Near-zero modes are found to have universal anti-correlations with monopoles below/above the critical β . In contrast to the result in QCD by Garcia-Garcia and Osborn, near-zero modes in the chiral restored phase are more delocalized than those in the chiral broken phase, which contradicts the Anderson-transition (AT) scenario for the chiral phase transition. We also study the nearest-neighbor level spacing distribution and find a signal of a Wigner-Poisson transition. We make a possible speculation on the chiral phase transition in 4D compact QED.

1 Introduction

Quantum ChromoDynamics(QCD) has many rich nonperturbative aspects and some of them still remain unsolved and challenging problems. The chiral symmetry breaking and the color confinement are the famous nonperturbative phenomena in QCD. Chiral symmetry, which is an approximate global symmetry in QCD, is spontaneously broken by nonperturbative dynamics of QCD. The broken chiral symmetry leads to large constituent quark masses of a few hundred MeV [1, 2, 3], which are responsible for about 99% of mass in the world, aside from some unknown factors such as dark matters.

The color confinement is brought about by the interquark potentials which linearly rise as interquark distances become large. This linearly rising potential implies the flux-tube formation among quarks [4, 5, 6, 7, 8], and the dual superconductor picture of the QCD vacuum [5, 6, 7, 8], in which QCD magnetic monopoles undergo condensation and color electric fields are squeezed into one-dimensional flux-tubes, is one of the most fascinating scenarios for the flux-tube formation.

The spontaneous chiral symmetry breaking is caused by non-zero chiral condensate $\langle \bar{\psi}\psi \rangle$, which is directly related to non-vanishing spectral density at the spectral origin of the Dirac operator, via the Banks-Casher relation [9]. The level dynamics of Dirac eigenvalues is then essential for the chiral phase transition. An Anderson-transition (AT) scenario for the chiral phase transition was recently proposed in Ref. [10]. The QCD vacuum undergoes a metal-insulator transition at the critical temperature, which causes a qualitative change in the level dynamics of Dirac eigenvalues. Instantons play an important role in the scenario.

A possible relationship between the chiral symmetry breaking and the color confinement is sometimes brought up for discussion because the chiral symmetry restoration and the confinement-deconfinement phase transition seem to take place at the same transition temperature or coupling. Though much effort has been made to clarify the possible relationship between them [11, 12, 13], we have no definite conclusion yet. The complicated QCD dynamics thwarts it.

*Yukawa Institute for Theoretical Physics, Kyoto university, Kitashirakawa-Oiwakecho, Sakyo, Kyoto 606-8502, Japan

Some of these features, the confinement and the spontaneous chiral symmetry breaking, can be also seen in compact QED in 1+3 dimensions. Compact QED has several properties in common with QCD. Compact QED in a strong-coupling region exhibits the charge confinement as well as the spontaneous chiral symmetry breaking. Its nature has been studied by many groups so far [14, 15, 16, 17, 18, 19, 20, 21, 22, 23, 24, 25, 26, 27, 28, 29, 30, 31, 32, 33, 34, 35, 36].

Then, compact QED can be considered as a possible testbed or as a model for a nonperturbative analysis of QCD. The key ingredient for the nonperturbative features in compact QED would be monopoles. Monopoles play essential roles in the charge confinement and its phase transition, and would play important roles also in the chiral symmetry breaking. As a matter of fact, neither the confinement nor the chiral symmetry breaking occurs without monopoles' degrees of freedom. Also in compact QED, the level dynamics of Dirac eigenvalues will play important roles in the chiral phase transition. In this paper, we mainly pay attention to the spatial distributions of low-lying Dirac eigenmodes in quenched compact QED, because the low-lying eigenvalue dynamics is considered to have a close connection with the low-lying eigenfunctions. We also investigate the spatial correlations between low-lying eigenfunctions and monopoles, the key player in the nonperturbative dynamics in compact QED.

The paper is organized as follows. We give the formalism employed in the present analysis in Sec. 2. In Sec. 3, the fundamental features of the low-lying Dirac modes are summed up. We show the lattice QED results in Sec. 4. Sec. 5 is devoted to the discussions and the speculations based on the present lattice QED results. We finally make a summary in Sec. 6.

2 Formalism

2.1 compact QED

The Wilson gauge action for compact QED is written as

$$S_{\text{QED}} = \beta \sum_x \sum_{\mu, \nu} (1 - \text{Re } P_{\mu\nu}(x)) \quad (1)$$

with link variables $U_\mu(x) \equiv e^{i\theta_\mu(x)} \in U(1)$ and plaquettes $P_{\mu\nu}(x) \equiv U_\mu(x)U_\nu(x + \hat{\mu})U_\mu^\dagger(x + \hat{\nu})U_\nu^\dagger(x)$. The constant $\beta \equiv \frac{1}{e^2}$ corresponds to the coupling constant. Here, the angle $\theta_\mu(x)$ ranges from $-\pi$ to π . Defining a plaquette angle $\theta_{\mu\nu}(x) \equiv \theta_\mu(x) + \theta_\nu(x + \hat{\mu}) - \theta_\mu(x + \hat{\nu}) - \theta_\nu(x) \in (-4\pi, 4\pi]$, S_{QED} is represented as

$$S_{\text{QED}} = \beta \sum_x \sum_{\mu, \nu} (1 - \cos \theta_{\mu\nu}(x)). \quad (2)$$

This compact formulation leads to several nonperturbative phenomena, such as the chiral symmetry breaking or the charge confinement at small β . Indeed, at zero temperature, compact QED has two phases; the confinement phase and the Coulomb phase. These two phases are separated with the critical value $\beta_c = 1.0111331(21)$ [33]. The system is in the confined phase at $\beta < \beta_c$, while it's in the Coulomb phase at $\beta > \beta_c$. The phase transition is weak first order.

In this paper, we employ $12^3 \times 12$ lattices at $\beta=0.99$, 1.01 and 1.03. We generate and investigate independent 48 gauge configurations at each β , which are generated with the standard Wilson gauge action imposing the periodic boundary conditions in all the directions. The system at $\beta=0.99$ (1.03) clearly lies in the confinement (Coulomb) phase, respectively, but the $12^3 \times 12$ system at $\beta=1.01$ is marginal. "Finite temperature" phase transition in compact QED was extensively investigated in Ref. [35], and the "transition temperature" $1/T$ at $\beta=1.01$ is found to be about $1/T \sim 6$. Then the $12^3 \times 12$ system at $\beta=1.01$ is considered to be just below the critical temperature and still in the confinement phase. The Polyakov loop defined as

$$P(\mathbf{x}) \equiv \int_0^\beta A_4(\mathbf{x}, t) dt = \prod_{t=0}^{N_t} U_4(\mathbf{x}, t) \quad (3)$$

can serve as an order parameter for the confinement-deconfinement phase transition in the quenched compact QED, which is zero in the confinement phase and shows a non-vanishing value in the deconfinement one. We plot the averaged values of Polyakov loops $|P|$ as well as

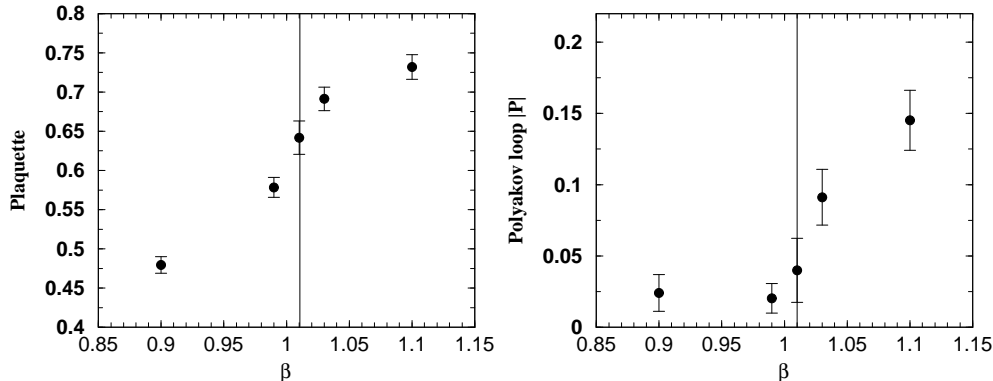


Figure 1: The left panel shows the averaged values of plaquettes and the right one denotes the averages of Polyakov loops at each β . The vertical line is drawn at $\beta=1.01$ for reference. The critical coupling β_c is 1.0111331(21).

the averages of plaquettes $P_{\mu\nu}(x)$ in Fig. 1. The horizontal axis denotes β in the figure. The vertical line is drawn at $\beta=1.01$ for reference. As expected, Polyakov loops $|P|$ tend to be zero at $\beta < \beta_c$ and to be finite at $\beta > \beta_c$. (We simply take the absolute values $|P|$ of Polyakov loops P and then they are always positive and real.) The signal of the phase transition is also found in the averaged values of plaquettes.

As we mentioned in Sec. 1, the key ingredient in compact QED in the confinement phase is monopoles' degrees of freedom. In order to extract monopoles, we divide plaquette angles $\theta_{\mu\nu}$ into two parts; physical fluxes $\bar{\theta}_{\mu\nu} \in (-\pi, \pi]$ and Dirac strings $2\pi n_{\mu\nu}$.

$$\theta_{\mu\nu} = \bar{\theta}_{\mu\nu} + 2\pi n_{\mu\nu} \quad (4)$$

$n_{\mu\nu} \in [0, \pm 1, \pm 2]$ is integer-valued and corresponds to the number of the Dirac strings penetrating the plaquette. We can now define the integer-valued DeGrand-Toussaint monopole current $m_\mu(x)$ [14] in a gauge-invariant manner;

$$m_\mu(x) = \frac{1}{2} \varepsilon_{\mu\nu\kappa\lambda} \Delta_\nu^+ n_{\kappa\lambda}(x), \quad (5)$$

where Δ_μ^\pm is a forward and backward derivative operator on a lattice, respectively. The monopole currents $m_\mu(x)$ satisfy the conservation law $\Delta_\mu^- m_\mu(x) = 0$ and hence form closed loops. We plot the averaged total lengths L_{mon} of monopoles in Fig. 2. The total monopole length quickly decreases around the critical coupling β_c .

Monopole currents can be unambiguously classified into monopole clusters C_{mon}^i . In Ref. [37], it was conjectured that the largest monopole cluster C_{mon}^1 occupies most of monopole currents and only the largest monopole cluster is relevant for the color confinement. In Fig. 3, we show the scattered plots of the numbers of the sites occupied by the i -th largest monopole cluster at each β , which are obtained with 48 configurations at each β . At $\beta=0.99$ and 1.01, we find prominently large monopole clusters of the length of about 10000, whereas we find no large cluster at $\beta=1.03$. The second largest cluster C_{mon}^2 is much smaller than the largest cluster C_{mon}^1 in the confinement phases, especially at $\beta=0.99$, which is the same tendency as that reported in Ref. [37]. This feature may indicate the possible interrelation between the nonperturbative

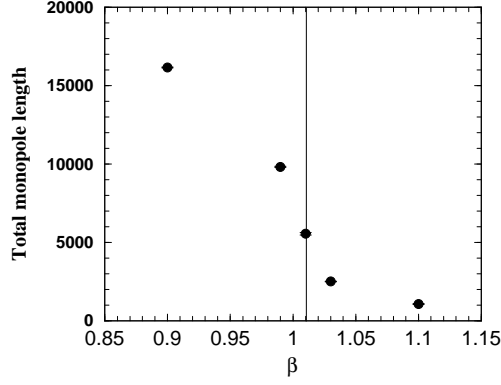


Figure 2: The total monopole length at each β . The vertical line is drawn at $\beta=1.01$ for reference. The critical coupling β_c is 1.0111331(21).

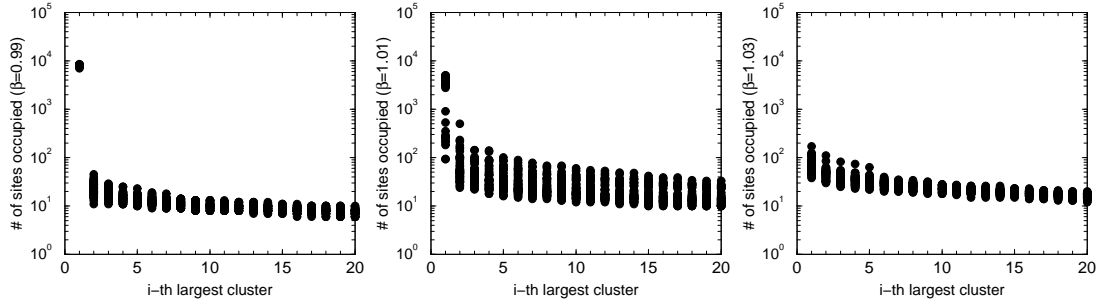


Figure 3: The numbers of the sites occupied by the i -th largest monopole cluster are plotted, which are obtained with 48 configurations at each β .

feature and the appearance of large monopole clusters also in compact QED. In other words, the nonperturbative dynamics could be characterized by the clustering-declustering feature of monopole loops.

2.2 Overlap fermion

For the fermion action, we employ the overlap formalism [38, 39]. The overlap-Dirac operator D is constructed as

$$D \equiv \rho[1 + \gamma_5 \text{sgn}(H_W)] \equiv \rho \left[1 + \gamma_5 \frac{H_W}{\sqrt{H_W^2}} \right] \quad (6)$$

and realizes the exact chiral symmetry on a lattice satisfying the Ginsparg-Wilson relation [40, 41]

$$\gamma_5 D + D \gamma_5 = \rho^{-1} D \gamma_5 D. \quad (7)$$

Here, $H_W \equiv \gamma_5(D_W - \rho)$ is the hermitian Wilson-Dirac operator defined with the standard Wilson-Dirac operator D_W . The “negative mass” ρ is chosen in the range of $0 < \rho < 2$, which we set 1.6 throughout this paper. We approximate the sign function $\text{sgn}(H_W)$ by 150 degrees’ Chebyshev polynomial [42], treating $\mathcal{O}(200)$ lowest eigenmodes of H_W exactly.

In order to check the locality of the overlap-Dirac operator, we investigate the norm $\|D(x, y)\eta(y)\|$ generated with a point-source η which has a support only on the single site x_0 . The exponential decay of $\|D(x, y)\eta(y)\|$ as the function of $|x - x_0|$ implies the locality of the overlap-Dirac

operator D [43]. We show in Fig. 4 $\|D(x, y)\eta(y)\|^2/\|D(x_0, y)\eta(y)\|^2$ logarithmically plotted as the function of $|x - x_0|$. The exponential decay can be actually found at all three β 's.

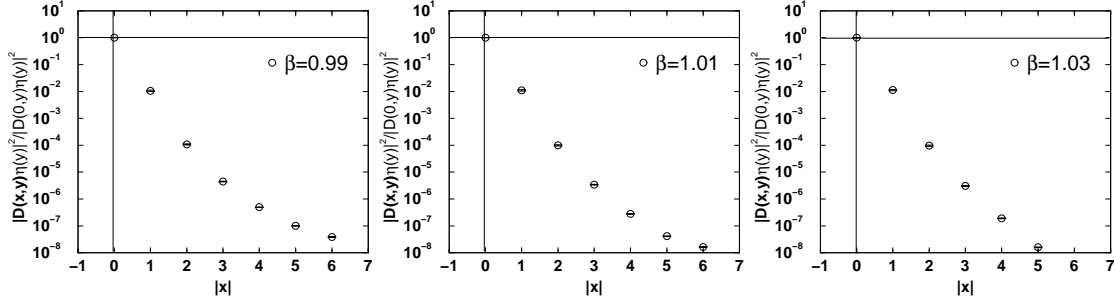


Figure 4: $\|D(x, y)\eta(y)\|^2/\|D(x_0, y)\eta(y)\|^2$ is logarithmically plotted as the function of $|x - x_0|$ at three different β 's. The horizontal and vertical lines are drawn for reference at $\|D(x, y)\eta(y)\|^2/\|D(x_0, y)\eta(y)\|^2 = 1$ and $|x - x_0| = 0$.

In the present analysis, we impose the periodic boundary conditions in all the spatial direction for the fermion fields, whereas the anti-periodic boundary condition is imposed in the temporal direction. We compute lowest 50 eigenpairs for each β implementing a restarted Arnoldi method [44]. All the eigenvalues λ_{lat} of D , which lie on a circle with the radius of ρ in a complex plain, are stereographically projected onto the imaginary axis via Möbius transformation [45],

$$\lambda = \frac{\lambda_{\text{lat}}}{1 - \lambda_{\text{lat}}/2\rho}. \quad (8)$$

3 Low-lying Dirac modes

We briefly survey the properties of Dirac eigenmodes in this section.

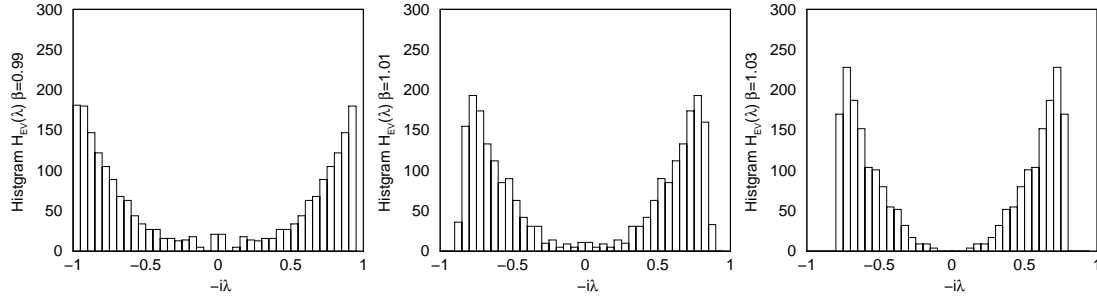


Figure 5: The histograms $H_{\text{ev}}(\lambda)$ of the eigenvalues λ of the overlap-Dirac operator D are plotted for each β . The horizontal axis denotes $-i\lambda$. All the eigenvalues λ_{lat} lying on a circle in a complex plain are stereographically projected onto the imaginary axis via Möbius transformation, $\lambda = \frac{\lambda_{\text{lat}}}{1 - \lambda_{\text{lat}}/2\rho}$.

First of all, we show the histograms $H_{\text{ev}}(\lambda)$ of Dirac eigenvalues in Fig. 7, where the horizontal axis denotes $-i\lambda$. Since a non-zero eigenvalue is always accompanied by its complex conjugate, the figure is symmetric about the H_{ev} axis. We find exact zero modes in the confinement phase at $\beta=0.99$ and 1.01 , but on the other hand no zero mode is seen in the Coulomb phase at $\beta=1.03$, which is consistent with the previous works [32, 34]. The numbers of zero modes found

	$\nu = 0$	$\nu = 1$	$\nu = 2$
$\beta = 0.99$	12	30	6
$\beta = 1.01$	32	12	4
$\beta = 1.03$	48	0	0

Table 1: The numbers of exact zero-modes found in 48 gauge configurations are listed. The i -th column gives the number of configurations with 0, 1, 2 zero-mode(s), respectively.

in 48 gauge configurations at each β are listed in Table. 1. The other prominent difference can be seen in the spectral density at the spectral origin. At the strong coupling ($\beta=0.99$ and 1.01), the density $\rho_{\text{ev}}(\lambda)$ of near-zero modes is rather dense, while it rapidly goes to zero at $\beta=1.03$ as $\sim |\lambda_{\text{ev}}|^3$. In other words, flattening of $H_{\text{ev}}(\lambda)$ at $\lambda \sim 0$ is observed at $\beta=0.99$ and 1.01. (We note that it is meaningless to directly compare the densities at the same λ among different couplings.) The non-vanishing eigenvalue density at $\lambda \sim 0$ is directly connected to non-zero chiral condensate via Banks-Casher relation [9] as

$$\langle \psi \bar{\psi} \rangle \propto \rho_{\text{ev}}(0). \quad (9)$$

This dense spectral density is then considered as a signal of the broken chiral symmetry in the strong-coupling compact QED. We note here that, strictly speaking, the spectral density just around the spectral origin is always zero in such a calculation, since a symmetry can never be spontaneously broken in a finite system.

We next extract the inverse participation ratio (IPR) for each eigenmode at each β . The IPR $I(\lambda)$ is defined as

$$I(\lambda) = V \sum_x \rho_{\text{IPA}}(x)^2, \quad \rho_{\text{IPR}}(x) \equiv \sum_{a,\alpha} |\psi_\lambda(x)|^2. \quad (10)$$

Here, V denotes the system volume and $\psi_\lambda(x)$ is the eigenfunction associated with an eigenvalue λ normalized as $\sum_x |\psi_\lambda(x)|^2 = 1$. The Roman and Greek alphabets a and α are the indices for a color and a spinor, respectively. The density $\rho_{\text{IPR}}(x)$ is obtained by locally summing up the absolute square of each component of an eigenfunction $\psi_\lambda(x)$ only over its color and spinor indices. The IPR is unity when $\psi_\lambda(x)$ maximally spreads over the system and equals to V in the case when $\psi_\lambda(x)$ lives only on a single site, reflecting the spatial distribution of the eigenfunction $\psi_\lambda(x)$.

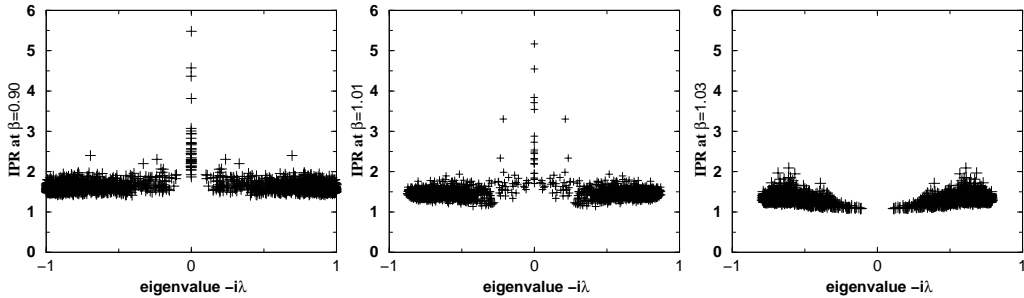


Figure 6: The scattered plots of inverse participation ratios of low-lying Dirac modes at $\beta=0.99$, 1.01 and 1.03. The horizontal axis denotes $-i\lambda$, the associated eigenvalue to each Dirac mode.

As one can see in Fig. 6, zero modes exhibit much larger IPRs than the other low-lying modes (near-zero modes). This tendency implies the stronger localization property peculiar to zero modes.

The IPRs for near-zero modes have β -dependence; the IPRs at larger β are smaller than those at smaller β as a whole, which implies that near-zero modes get delocalized as we increase β . This delocalization property of near-zero modes was also found in Ref. [34]. The localization-delocalization properties of near-zero modes, which are associated with near-zero Dirac eigenvalues, would have some concerns with the chiral phase transition.

4 Histograms of Dirac eigenmodes

The IPR surely reflects one aspect of a spatial distribution of an eigenfunction. However, it can say almost nothing about the “shape” of an eigenmode. The difficulty in such an analysis comes from the difficulty in a quantitative evaluation of the detail of eigenfunction distributions.

We, at the moment, concentrate ourselves on the eigenfunction-density histograms $H_\psi^{\text{all}}(\rho_\psi)$ counted over all the sites in the system. The density $\rho_\psi \equiv \rho_{\text{IPR}}$ here is merely the same quantity as the IPR density ρ_{IPR} of a Dirac eigenfunction $\psi_\lambda(x)$. If an eigenfunction is quite strongly localized, H_ψ^{all} for it will have two peaks at $\rho_\psi \sim 0$ and at large ρ_ψ . (The peak at $\rho_\psi \sim 0$ is much higher.) On the other hand, if an eigenfunction maximally spreads over the system, H_ψ^{all} will have a single and shape peak at $\rho_\psi \sim 1/V \sim 0.00005$, because each eigenfunction is normalized as $\sum_x \rho_{\text{IPR}} = 1$.

The open bars in Fig. 7 show the typical density histograms H_ψ^{all} for both zero and near-zero modes at $\beta=0.99, 1.01$ and 1.03 . The histograms H_ψ^{all} for zero modes at $\beta=0.99$ and 1.01 have a relatively long tail at large ρ_ψ and show a large height at $\rho_\psi \sim 0$ compared to those of near-zero modes, which also exhibits the stronger localization property of zero modes. The peak position of H_ψ^{all} for near-zero modes seems to be shifted to larger ρ_ψ than those for zero modes, which is a signal of a weaker localization or non-localization property.

Our main concern is a relationship between Dirac modes and monopoles. We next investigate another type of histogram $H_\psi^{\text{mon}}(\rho_\psi)$, which is defined by counting only ρ_ψ “on monopoles”. H_ψ^{mon} is here normalized as $\int_0^\infty H_\psi^{\text{mon}}(t)dt = \int_0^\infty H_\psi^{\text{all}}(t)dt$. Since only the large monopole clusters seem essential for the nonperturbative phenomena, such as the confinement or the chiral symmetry breaking, we classify monopole clusters into two categories; the large-cluster group $\mathcal{C}_{\text{mon}}^L \equiv \{C_{\text{mon}}^i (i \leq N_{\text{thr}})\}$ and the small-cluster group $\mathcal{C}_{\text{mon}}^S \equiv \{C_{\text{mon}}^i (i > N_{\text{thr}})\}$. We simply determine N_{thr} so that $|C_{\text{mon}}^{N_{\text{thr}}}| = 20$, with $|C_{\text{mon}}^i|$ the size of the i -th largest cluster C_{mon}^i . Taking into account that monopoles are by definition located at the intermediate points $\bar{x} \equiv x + (1/2, 1/2, 1/2, 1/2)$, ρ_ψ ’s are simply redefined by averaging them around intermediate points \bar{x} as

$$\rho_\psi \rightarrow \rho_\psi(\bar{x}) \equiv \sum_{|x-\bar{x}|=1} \rho_\psi(x)/2^4 \quad (11)$$

In the case when there is no correlation between the spatial fluctuations of Dirac modes and monopole distributions, H_ψ^{mon} and H_ψ^{all} would coincide with each other. In Fig. 7, we show the histograms H_ψ^{mon} for both zero and near-zero modes counted on $\mathcal{C}_{\text{mon}}^L$ (large monopole cluster) at $\beta=0.99, 1.01$ and 1.03 as solid lines. The histograms H_ψ^{mon} for zero modes as well as those for near-zero modes show little difference from H_ψ^{all} , when viewed as a whole. However, at small ρ_ψ , we can find a remarkable difference for near-zero modes at all three β ’s. At $\rho_\psi < 0.00005$, the histogram H_ψ^{mon} counted only on large-cluster monopoles takes a larger value than H_ψ^{all} counted over all the sites. On the other hand, at $\rho_\psi > 0.00005$, H_ψ^{mon} tends to be smaller than H_ψ^{all} . This tendency indicates that monopoles “run” on the sites where the density ρ_ψ of Dirac eigenfunctions is small. Or we can say that near-zero Dirac modes are localized avoiding monopoles.

We define and investigate the histogram ratios $R_\psi^{L,S}(\rho_\psi)$ in order to evaluate the correlations

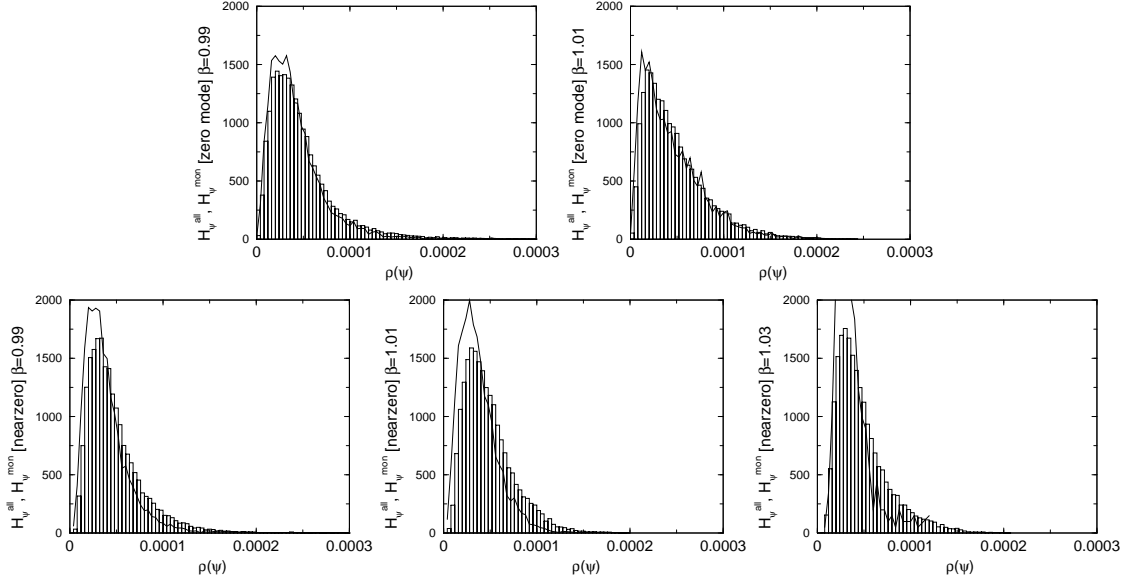


Figure 7: The density histograms H_{ψ}^{all} and H_{ψ}^{mon} are plotted as the function of ρ_{ψ} . The upper panels are for zero modes at $\beta=0.99$ and 1.01 and the lower ones for near-zero modes at $\beta=0.99$, 1.01 and 1.03. The histograms H_{ψ}^{all} , which are counted over all the site, are shown as open bars. The histograms H_{ψ}^{mon} , which are counted only on the large monopole clusters, are shown as solid lines.

in a semi-quantitative way;

$$R_{\psi}^L(\rho_{\psi}) \equiv \frac{H_{\psi}^{\text{mon}}(\rho_{\psi})}{H_{\psi}^{\text{all}}(\rho_{\psi})} \times \frac{V}{\sum_{i \leq N_{\text{thr}}} |C_{\text{mon}}^i|}, \quad (12)$$

$$R_{\psi}^S(\rho_{\psi}) \equiv \frac{H_{\psi}^{\text{mon}}(\rho_{\psi})}{H_{\psi}^{\text{all}}(\rho_{\psi})} \times \frac{V}{\sum_{i > N_{\text{thr}}} |C_{\text{mon}}^i|}. \quad (13)$$

Here $\sum_i |C_{\text{mon}}^i|$ is the sum of the volumes $|C_{\text{mon}}^i|$ the i -th largest monopole clusters C_{mon}^i occupy, and N_{thr} is fixed so that $|C_{\text{mon}}^{N_{\text{thr}}}| = 20$ at all three β 's. This quantity $R_{\psi}^{L,S}(\rho_{\psi})$ equals to 1, *if there is no correlation between the spatial fluctuations of Dirac modes and monopoles*. In the case when a positive (negative) correlation exists between the spatial fluctuations of Dirac modes and monopoles, $R_{\psi}^{L,S}(\rho_{\psi}) > 1$ at smaller (larger) ρ_{ψ} and $R_{\psi}^{L,S}(\rho_{\psi}) < 1$ at large (smaller) ρ_{ψ} hold.

In Fig. 8 and 9, we plot the histogram ratios $R_{\psi}^L(\rho_{\psi})$ and $R_{\psi}^S(\rho_{\psi})$, respectively, for both zero and near-zero modes at $\beta=0.99$, 1.01 and 1.03. (Meanwhile, for the $R_{\psi}^{L,S}(\rho_{\psi})$ for near-zero modes, we simply average R over all the available near-zero modes.) Solid lines at $\rho_{\psi} = 0.0002$ and at $R_{\psi}^L(\rho_{\psi}) = 1$ are drawn for reference. In these figures, one may find that R_{ψ}^L and R_{ψ}^S all go to zero at larger ρ_{ψ} . However, this tendency should be taken with a grain of salt, because histograms H_{ψ}^{all} are quite sparse at $\rho_{\psi} > 0.0002$ and this simple analysis cannot be reliable. In fact, unnatural kinks are seen around $\rho_{\psi} \sim 0.0002$. Then, we should evaluate R_{ψ}^L and R_{ψ}^S only with $\rho_{\psi} < 0.0002$. The ratios (to 1) of the squared norms of the Dirac modes obtained by summing up only ρ_{ψ} larger than 0.0002 are 12(7)%, 15(11)%, 1.4(3)%, 0.5(3)%, 0.1(1)% for zero modes at $\beta=0.99$, 1.01, and 1.03, respectively. We summarize the ratios in Table. 2. As expected from the localization property of zero modes, their ratios are larger than those of near-zero modes. In spite of the truncation at $\rho_{\psi} \sim 0.0002$,

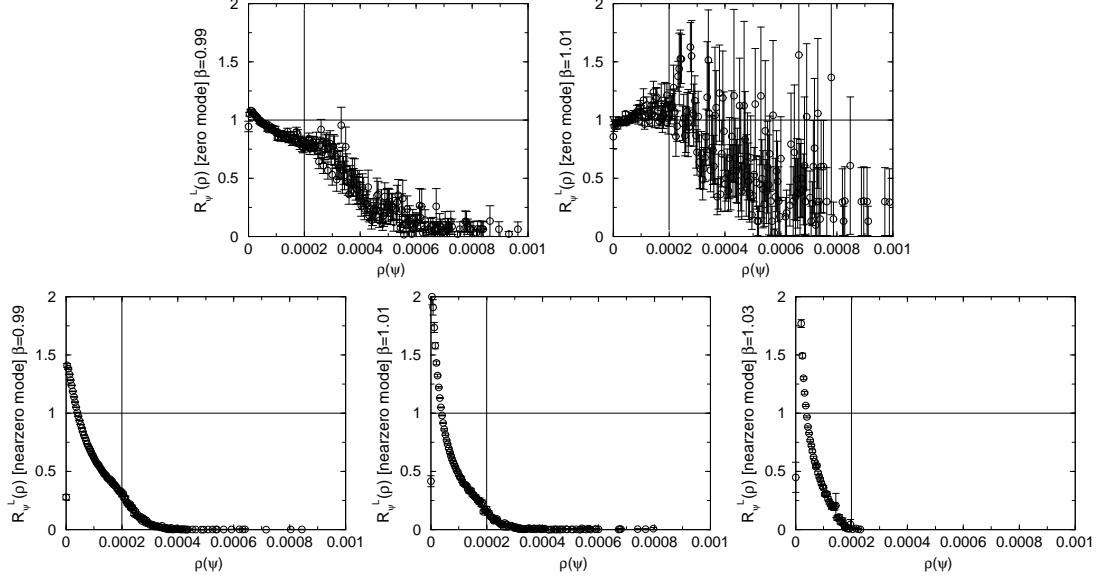


Figure 8: The histogram ratios $R_{\psi}^L(\rho_{\psi})$ for zero (upper two panels) and near-zero modes (lower three panels) at $\beta=0.99, 1.01$ and 1.03 are plotted. We draw two lines at $\rho_{\psi} = 0.0002$ and $R_{\psi}^L(\rho_{\psi}) = 1$ for reference.

	$\beta = 0.99$	$\beta = 1.01$	$\beta = 1.03$
zero modes	12(7)%	15(11)%	-
near-zero modes	1.4(3)%	0.5(3)%	0.1(1)%

Table 2: The ratios (to 1) of the squared norms of the Dirac eigenmodes evaluated only with $\rho_{\psi} > 0.0002$.

the analysis in the range of $\rho_{\psi} < 0.0002$ might be enough to grasp the nature of Dirac modes, at least for near-zero modes, since $\rho_{\psi} > 0.0002$ are responsible only for a few % of the total squared norms.

Fig. 10 and 11 again show the histogram ratios $R_{\psi}^L(\rho_{\psi})$ and $R_{\psi}^S(\rho_{\psi})$ plotted in the range of $\rho_{\psi} < 0.0002$, respectively, for both zero and near-zero modes at $\beta=0.99, 1.01$ and 1.03 .

4.1 Results for zero Dirac modes

While we have only a few dozen of zero modes in 48 gauge configurations and the statistical errors are consequently rather large, the spatial fluctuations of zero modes seem to have no remarkable correlation with either large (Fig. 10) or small (Fig. 11) monopole clusters, which you can see in upper two panels in Figs. 10, 11. There are naively three possibilities: 1)The eigenfunctions fluctuate in a complicated way forming multifractal structures, but they are completely smeared out through the redefinition in Eq. 11, which leads to the apparent absence of correlations. 2)The eigenfunctions are not completely smeared out in Eq. 11, and the fluctuations are still complicated, which also leads to the apparent absence of correlations. 3)They simply have little correlation with monopoles.

In order to verify the possibility 1) or 2), it is needed to compute multifractal dimensions of the modes by analyzing the scaling of eigenfunction moments. Large monopole clusters in fact occupy almost half of the total volume of $12^3 \times 12 = 20736$ and their structures themselves

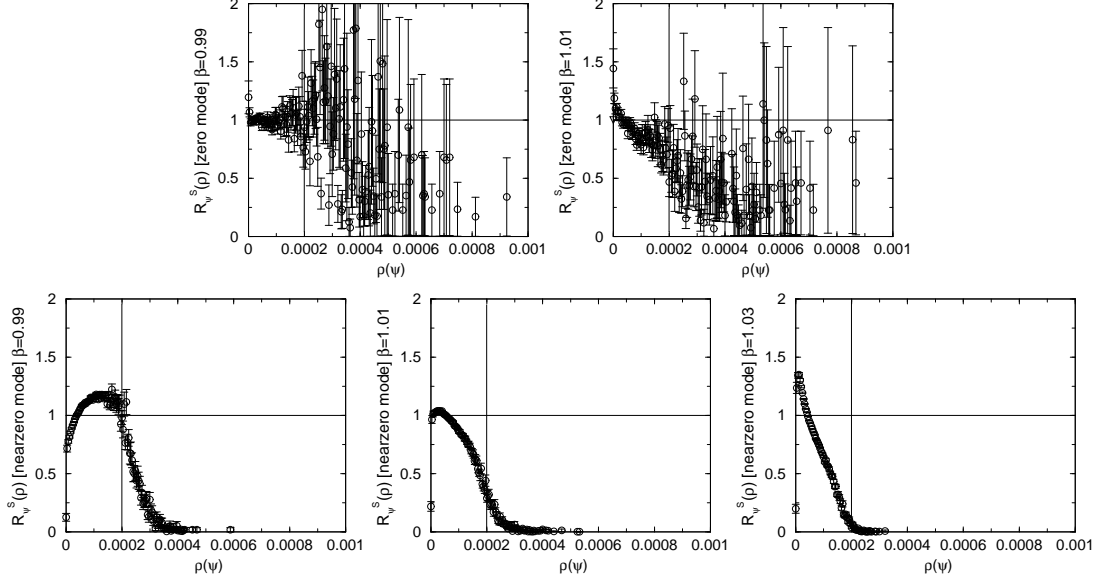


Figure 9: The histogram ratios $R_{\psi}^S(\rho_{\psi})$ for zero (upper two panels) and near-zero modes (lower three panels) at $\beta=0.99$, 1.01 and 1.03 are plotted. We draw two lines at $\rho_{\psi} = 0.0002$ and $R_{\psi}^L(\rho_{\psi}) = 1$ for reference.

are complicated. Then, the eigenfunction distributions would look complex and would be easily smeared, even if there exist clear (anti-)correlations with monopoles. We unfortunately employ only $12^3 \times 12$ lattices at present and the scaling analysis is left for further study.

In the case of 3), there's nothing special. However, taking into account that zero modes are strongly localized and that the histogram $H_{\psi}(\rho_{\psi})$ still has non-zero values even at much larger ρ_{ψ} , $H_{\psi}(\rho_{\psi})$ at large ρ_{ψ} may have important information of Dirac zero modes. In fact, the squared norm of a zero mode carried by $\rho_{\psi} > 0.0002$, which we have discarded, reach O(10)% of the total squared norm. In Ref. [46], the authors conjectured that Dirac zero modes mainly appear at the intersections of vortexes. Our present analysis cannot reveal the correlations between the intersections and zero modes, due to the simpleness of our analysis and the discard of $\rho_{\psi} > 0.0002$. We need more statistics and detailed analyses in order to make definite conjectures upon zero modes.

4.2 Averaged results for near-zero Dirac modes

As for near-zero Dirac modes and large monopole clusters, one can see the outstanding anti-correlation in Fig. 10. The histogram ratio $R_{\psi}^L(\rho_{\psi})$ is clearly larger than 1 at small ρ_{ψ} and less than 1 at large ρ_{ψ} beyond the statistical errors. Although the values of $R_{\psi}^L(\rho_{\psi})$ themselves are slightly different among three β 's, $\beta=0.99$, 1.01 and 1.03, the bulk properties are surely the same, which means the existence of the universal anti-correlations between near-zero Dirac modes and large monopole clusters around the critical coupling β_c .

On the other hand, $R_{\psi}^S(\rho_{\psi})$ for $\beta=0.99$, 1.01 and 1.03 in Fig. 11 show three different behaviors. One may find a weak positive correlation between Dirac near-zero modes and small monopole clusters at $\beta=0.99$, whereas anti-correlations can be found at $\beta=1.01$ and 1.03. This tendency might be the consequence of the anti-correlation between the modes and large monopole clusters. In fact, at $\beta=0.99$, the sizes of the small monopole clusters are much smaller than those at $\beta=1.03$, which you can see in Fig. 3, and they would not contribute to the infrared dynamics

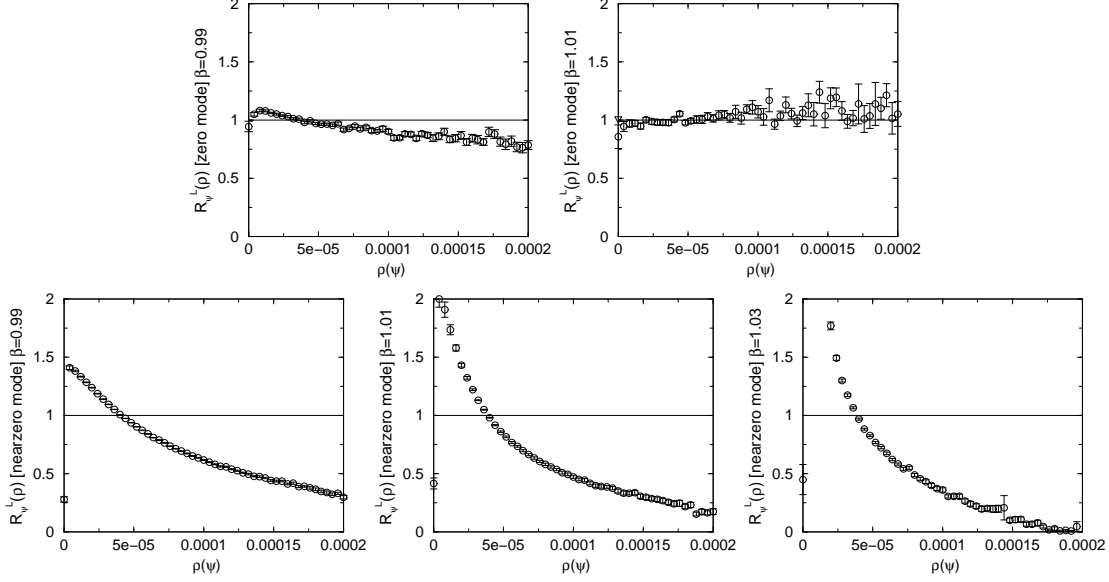


Figure 10: The histogram ratios $R_{\psi}^L(\rho_{\psi})$ for zero (upper two panels) and near-zero modes (lower three panels) at $\beta=0.99, 1.01$ and 1.03 are plotted in the range of $0 \leq \rho_{\psi} \leq 0.0002$. We draw a line at $R_{\psi}^L(\rho_{\psi}) = 1$ for reference.

of compact QED. If it is the case, the Dirac near-zero modes are displaced by large monopole clusters “onto” small clusters, which gives rise to the “apparent positive correlation” seen in $R_{\psi}^S(\rho_{\psi})$ at $\beta=0.99$.

4.3 Results for near-zero Dirac modes ($|\lambda| < 0.3$, just around the spectral origin)

We have shown $R_{\psi}^{L,S}(\rho_{\psi})$ for zero modes as well as $R_{\psi}^{L,S}(\rho_{\psi})$ averaged on all the available near-zero modes for each β . We pay special attention to the near-zero modes lying just around the spectral origin in this subsection. They seem to have rather different features from the other near-zero modes. For example, one can find much smaller IPRs, which are almost 1, around the spectral origin at $\beta=1.03$.

In Fig. 12 and 13, we plot the histogram ratios $R_{\psi}^L(\rho_{\psi})$ and $R_{\psi}^S(\rho_{\psi})$, respectively, for the near-zero modes lying just around the spectral origin at $\beta=0.99, 1.01$ and 1.03 . Solid lines at $R_{\psi}^{L,S}(\rho_{\psi}) = 1$ are drawn for reference. We find that $R_{\psi}^L(\rho_{\psi})$ and $R_{\psi}^S(\rho_{\psi})$ at $\beta=0.99$ and 1.01 are rather close to 1 and indicate weak anti-correlations with monopoles, in contrast to $R_{\psi}^L(\rho_{\psi})$ and $R_{\psi}^S(\rho_{\psi})$ at $\beta=1.03$, which show clear and much stronger anti-correlations with monopoles. The spatial fluctuations of just-near-zero modes at $\beta=0.99$ and 1.01 seem to have little correlation with monopoles. We can again speculate the same three reasons as listed in Sec. 4.1: 1)The eigenfunctions fluctuate in a complicated way forming multifractal structures, but they are rather smeared out through the redefinition in Eq. 11, which leads to the apparent weakness of correlations. 2)The eigenfunctions are not completely smeared out in Eq. 11, and the fluctuations are still complicated, which also leads to the apparent weakness of correlations. 3)They simply have a weak correlation with monopoles.

Considering that the anti-correlation between eigenfunction fluctuations and monopoles at $\beta=1.03$ is quite irrefragable, the possibility 3) may not be likely. Multifractality or complexity of the near-zero modes just around the spectral origin would again weaken apparent correlations

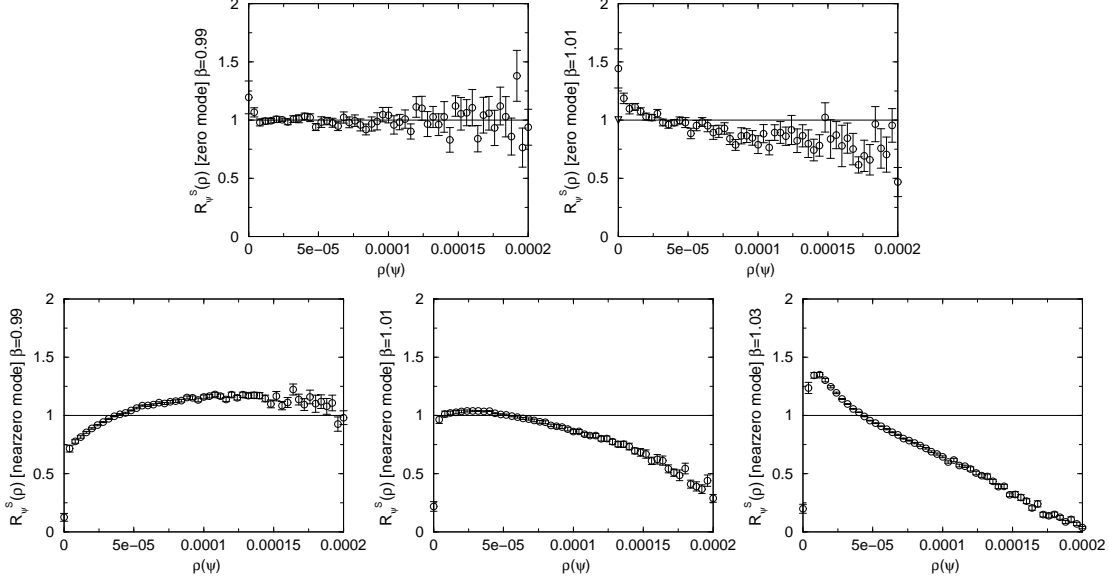


Figure 11: The histogram ratios $R_{\psi}^S(\rho_{\psi})$ for zero (upper two panels) and near-zero modes (lower three panels) at $\beta=0.99, 1.01$ and 1.03 are plotted in the range of $0 \leq \rho_{\psi} \leq 0.0002$. We draw a line at $R_{\psi}^L(\rho_{\psi}) = 1$ for reference.

with monopoles in the present analysis. Let us here assume that a just-near-zero mode whose eigenvalue satisfy $|\lambda| < 0.3$ is equally distributed on the sites without any monopoles, which corresponds to the case when there exists a very strong anti-correlation between just-near-zero modes and monopoles. In that case, the IPRs should be 2, 1.43 and 1.14 at $\beta=0.99, 1.01$ and 1.03 , respectively, because the monopole lengths are $\sim 10000, \sim 6000$ and ~ 2500 at $\beta=0.99, 1.01$ and 1.03 . The real IPRs for the just-near-zero modes at $\beta=0.99, 1.01$ and 1.03 are $1.75(17), 1.65(35)$ and $1.16(5)$, which are rather close to the “estimated” values, 2, 1.43 and 1.14. Although this estimation should be discounted, the existence of the anti-correlations between eigenfunction fluctuations and monopoles, at least, does not contradict the IPRs observed in the present lattice calculations.

In any case, the anti-correlation between near-zero Dirac modes and large monopole-clusters seems to exist. The important point is the universality of the anti-correlation between near-zero modes and large monopole clusters. This simple rule does not drastically change before/after the phase transition. Near-zero modes are “scattered” by monopole clusters.

5 Discussions and Speculations

5.1 Dirac eigenvalues and Chiral condensate

As we have seen in Sec. 3, Dirac eigenvalues have non-vanishing density $\rho_{\text{ev}}(0)$ at the spectral origin in the chiral broken phase, and this non-vanishing value is directly connected to the non-zero chiral condensate $\langle \bar{\psi}\psi \rangle$ via the Banks-Casher relation. The non-vanishing $\rho_{\text{ev}}(0)$ is generated by the “repulsive force” among the eigenvalues: The eigenvalues of the overlap-Dirac operator lying on the circumference of the circle in a complex plane repel each other, and consequently near-zero eigenvalues are pushed towards the spectral origin forming the non-zero $\rho_{\text{ev}}(0)$. Namely, the driving force of the chiral symmetry breaking is the “repulsive force” among Dirac eigenvalues. On the other hand, when $\rho_{\text{ev}}(0)$ is zero, the repulsive force is considered to

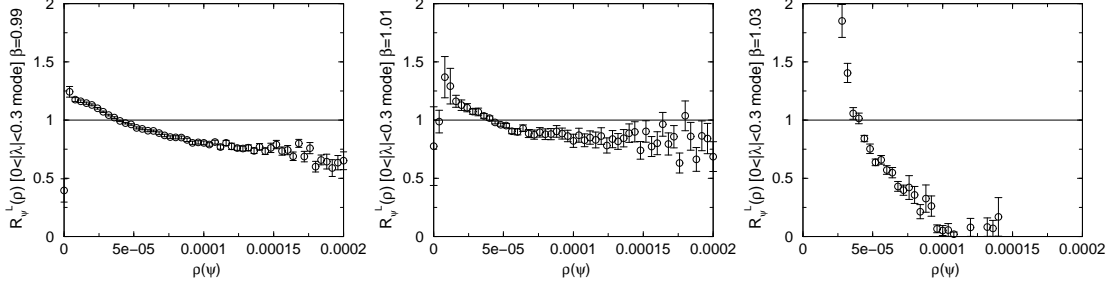


Figure 12: The histogram ratios $R_\psi^L(\rho_\psi)$ for the near-zero modes, whose associated eigenvalues satisfy $0 < |\lambda| < 0.3$, at $\beta=0.99, 1.01$ and 1.03 , are plotted in the range of $0 \leq \rho_\psi \leq 0.0002$. We draw a line at $R_\psi^L(\rho_\psi) = 1$ for reference.

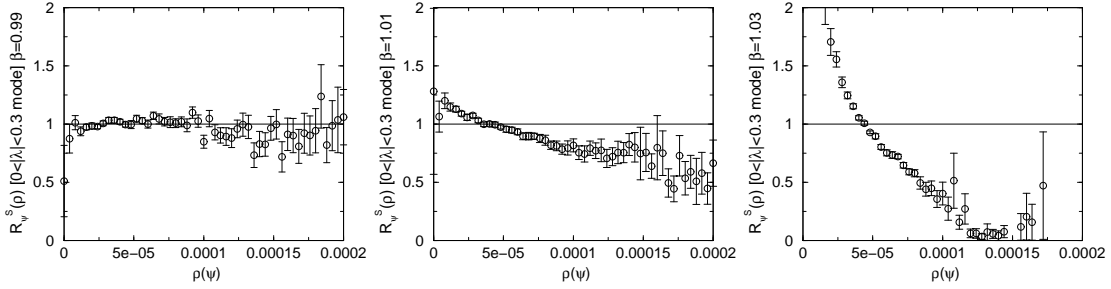


Figure 13: The histogram ratios $R_\psi^S(\rho_\psi)$ for the near-zero modes, whose associated eigenvalues satisfy $0 < |\lambda| < 0.3$, at $\beta=0.99, 1.01$ and 1.03 , are plotted in the range of $0 \leq \rho_\psi \leq 0.0002$. We draw a line at $R_\psi^L(\rho_\psi) = 1$ for reference.

be weaker or zero. The magnitude of this force can be revealed by level statistics.

We show in Fig. 14 the unfolded nearest-neighbor level spacing distributions $P_{\text{lat}}(s)$ of the low-lying Dirac eigenvalues obtained at $\beta=0.99, 1.01$ and 1.03 . The solid lines denote the Wigner distribution function $P_{\text{Wig}}(s) \equiv \frac{32}{\pi^2} s^2 \exp(-\frac{4}{\pi} s^2)$ and the dashed lines the Poisson distribution function $P_{\text{Poi}}(s) = \exp(-s)$. The Wigner distribution function $P_{\text{Wig}}(s)$ is a good approximation of the original distribution function obtained by the random matrix theory (RMT) for the chiral unitary ensemble (chUE). The Poisson distribution $P_{\text{Poi}}(s)$ appears, for example, in the system where eigenenergy levels have *no correlation* with each other.

The level spacing distributions $P_{\text{lat}}(s)$ at $\beta=0.99$ and 1.01 show the good coincidence with $P_{\text{Wig}}(s)$, which you can find in the left and the middle panels in Fig. 14. The manifestation of the Wigner distribution, at $\beta=0.99$ and 1.01 in the chiral broken phase, implies the level repulsion among the low-lying eigenvalues, which is consistent with the non-vanishing eigenvalue density $\rho_{\text{ev}}(0)$ at the spectral origin. On the other hand, at $\beta=1.03$ in the chiral restored phase, $P_{\text{lat}}(s)$ coincides with neither the Wigner distribution $P_{\text{Wig}}(s)$ nor the Poisson distribution $P_{\text{Pos}}(s)$. $P_{\text{lat}}(s)$ at $\beta=1.03$ seems to be on the way from the Wigner to the Poisson distribution. As a remarkable fact, you can find the long tail of $P_{\text{lat}}(s)$ stretching even at $s = 4$. This tendency seen at $\beta=1.03$ shows a weaker repulsion among the low-lying eigenvalues than at $\beta=0.99$ and 1.01 , which leads to small or zero eigenvalue density $\rho_{\text{ev}}(0)$ at the spectral origin. The Wigner-Poisson transition in the nearest-neighbor level spacing of the low-lying Dirac eigenvalues appears at $\beta > 1.01$, almost at the same time as the confinement-deconfinement phase transition. Such a Wigner-Poisson transition was also observed in Ref. [10], where the authors investigated the

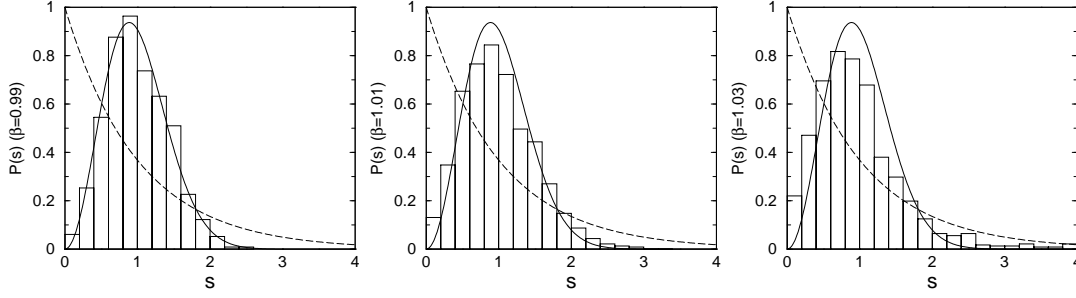


Figure 14: The unfolded nearest-neighbor level spacing distributions $P_{\text{lat}}(s)$ at $\beta = 0.99, 1.01$ and 1.03 . The solid lines denote the Wigner distribution function $P_{\text{Wig}}(s) \equiv \frac{32}{\pi^2} s^2 \exp(-\frac{4}{\pi} s^2)$ and the dashed lines the Poisson distribution function $P_{\text{Poi}}(s) = \exp(-s)$.

neighboring level spacing in finite-temperature QCD with the staggered fermion. The level dynamics of low-lying Dirac modes around the chiral phase transition in compact QED and QCD seem to coincide with each other.

For QCD and compact QED, the level spacing distributions were also investigated in Refs. [31, 47, 48], in terms of the realization of quantum chaos in gauge theories. We note that our observations are somewhat inconsistent with them. In Refs. [31, 47, 48], no sign for a transition to the Poisson distribution is found even at $\beta=1.10$, which corresponds to the clearly deconfined phase, and the authors claimed that the deconfinement phase transition did not seem to coincide with a transition in the level spacing distribution. The inconsistency might come from the different setups in the analyses. We investigated the level spacing of the only 50 low-lying Dirac eigenvalues employing the overlap formalism and the larger lattices, while the authors in Refs. [31, 47, 48] investigated the nearest-neighbor level spacing of the bulk of the eigenvalues with the staggered fermion.

So far, we have mainly shown the numerical facts obtained in the present analysis. In the next subsection, we make a possible speculations about the chiral transition mechanism in compact QED.

5.2 Possible speculations

We have found the sign of a Wigner-Poisson transition in the neighboring level spacing distributions of the low-lying Dirac eigenmodes. Although this transition in the level spacing seems consistent with that found in QCD [10], the mechanisms seem different from each other. The authors in Ref. [10] claimed the metal-insulator transition as the Anderson transition (AT) [49] of the QCD vacuum in the chiral phase transition. In fact, they found the strong localization property of low-lying Dirac eigenfunctions around the spectral origin above the transition temperature. However, the IPRs of the low-lying modes at $\beta=1.03$ in Fig. 6, especially around the spectral origin, are much smaller than those at $\beta=0.99$ and 1.01 , which implies the delocalization property of the modes in the chiral restored phase in compact QED. Our result contradicts the AT scenario. Such a difference may come from the dimensionality. While we have investigated isotropic 4D systems, the finite temperature systems were investigated in Ref. [10], whose dimensionality is reduced by “finite temperature effect”. Such contributions can be revealed by studying the “finite temperature” compact QED systems with the same setup as the present study.

The Wigner/Poisson distributions in neighboring level spacing distributions can be also found in classically chaotic/regular systems. Berry and Tabor [50] drew the conclusion that in a classically integrable system with more than one degree of freedom the level spacing distribution

of quantum spectra obeys the Poisson distribution. We can also find in Ref. [51] the famous conjecture by Bohigas, Giannoni and Schmit stating that the level statistics of a quantum system whose classical counterpart is chaotic do not show a dependence on the details of the dynamics but depend only on the global symmetry of the system. Level statistics in such a system coincide with those obtained by the random matrix theory with the same global symmetry. (This conjecture is not always true. A quantum kicked rotor does not satisfy the conjecture.)

For the classical lattice Yang-Mills theory, the authors in Ref. [52] computed the complete Lyapunov spectrum and found that Yang-Mills fields are strongly chaotic at all energies. The gauge configurations corresponding to the deconfinement phase were found to be still chaotic though they are less chaotic than in the strong coupling phase at finite temperature [53]. In Ref. [54], the authors analyzed the nearest-neighbor spacing distribution in the spatially homogeneous SU(2) Yang-Mills-Higgs system and found the signature of a Wigner-Poisson transition in accordance with the value of the Higgs field in the vacuum. The spatially homogeneous Yang-Mills Chern-Simons Higgs system was also investigated in Ref. [55]. For the fermion sector, no signal for a Wigner-Poisson transition in level spacing distributions was reported in Refs. [31, 47, 48].

In the previous subsection, we have found the sign of a Wigner-Poisson transition in the level spacing of the low-lying Dirac eigenvalues, but have found no clear signal of the localization of low-lying modes in the chiral restored phase, which clearly contradicts the AT or metal-insulator-transition scenario for the phase transition [10]. (The contradiction may originate from the difference in dimensionality.) Then, is it the possible sign of a chaotic-regular transition in compact QED? If yes, what is responsible for the transition? The key player might be monopoles. As was seen in Sec. 4, there exist universal anti-correlations between monopoles and near-zero Dirac eigenmodes. In the system where large monopole clusters exist, the near-zero modes are “scattered” by monopoles in a very complicated way, which results in the Wigner distribution of the level spacing. When there exist only small monopole clusters in a system, this complexity is weakened and the system is less chaotic. The level dynamics of low-lying Dirac eigenvalues are controlled by monopoles’ clustering-declustering feature.

If it happens to be the case, the confinement-deconfinement transition and the chiral phase transition in compact QED can be closely related through monopoles. On one hand, the monopoles’ clustering-declustering feature is surely responsible for the confinement-deconfinement transition. On the other hand, the monopoles’ clustering-declustering transition gives rise to the change in the level dynamics of low-lying Dirac eigenmodes through the possible chaotic-regular transition of the system, which leads to the change in the eigenvalue density at the spectral origin, or equivalently in the chiral condensate $\langle\bar{\psi}\psi\rangle$.

One may wonder whether the complexity in the strong coupling QED system comes mainly from monopoles or simply from gauge fields’ fluctuations. To verify it, the use of cooled gauge configurations is of advantage. It was reported in Ref. [56], that patterns in the eigenvalue spectrum, characteristic are conserved to a large degree even in cooled configurations, at least in SU(2) quenched lattice gauge theory. It implies that the spontaneous chiral symmetry breaking is not caused by local structures of the vacuum but caused by global structures or objects such as instantons. The study based on the use of cooled configurations is left for further study.

Though what we have found is only a Wigner-Poisson transition in the neighboring level spacing of Dirac low-lying modes and we have shown no definite evidence for “chaos for fermions”, it is likely that the “scattering” by monopoles gives rise to the complex quantum interference of Dirac low-lying modes and causes the critical behavior of low-lying Dirac modes in compact QED.

6 Summary

We have mainly studied the correlations between the fluctuations of low-lying Dirac eigenfunctions and monopoles in quenched compact QED at $\beta=0.99, 1.01$ and 1.03 , employing $12^3 \times 12$ lattices and the overlap formalism for the fermion.

We have found that the nearest-neighbor level spacing distribution coincides with the Wigner distribution at $\beta = 0.99, 1.01 < \beta_c$, and that it seems to be on the way from the Wigner to the Poisson distribution at $\beta = 1.03 > \beta_c$, which is consistent with the non-vanishing (vanishing) spectral density at the spectral origin or equivalently the non-vanishing (vanishing) chiral condensate at $\beta < \beta_c$ ($\beta > \beta_c$).

Near-zero modes have been found to have universal anti-correlations with monopoles below/above the critical β , though those just around the spectral origin show a little different behavior: The fluctuations of near-zero eigenfunctions just around the spectral origin at $\beta < \beta_c$ seem to have a relatively small correlation with monopoles, whereas those at $\beta > \beta_c$ have a strong anti-correlation. The small correlation of just-near-zero modes at $\beta < \beta_c$ may indicate their complex fluctuations in the vacuum and does not yet deny the universality of the anti-correlation. In any case, there seem to exist anti-correlations between near-zero modes and monopoles. Near-zero modes are “scattered” by monopoles in compact QED, which is considered as the origin of the critical behaviors of low-lying Dirac eigenmodes.

In contrast to the results in Ref. [10], near-zero modes in the chiral restored phase are more delocalized than those in the chiral broken phase showing small IPRs of almost 1, which contradicts the AT scenario for the chiral phase transition proposed in Ref. [10]. The chiral phase transition in 4D compact QED might be associated with the chaotic-regular transition of the vacuum, which is brought about by the clustering-declustering feature of monopoles. If it is the case, the chiral phase transition and the confinement-deconfinement transition are still and simply the consequences of the clustering-declustering transition of monopoles.

acknowledgments

The author thanks T. Kunihiro, H. Matsufuru, T. Onogi and K. Totsuka for helpful comments, and is supported by the Japan Society for the Promotion of Science for Young Scientists. All the numerical calculations in the paper were carried out on NEC SX-8 at the Yukawa Institute Computer Facility.

References

- [1] A. De Rujula, H. Georgi and S. L. Glashow, Phys. Rev. D **12**, 147 (1975).
- [2] Y. Nambu and G. Jona-Lasinio, Phys. Rev. **124** (1961) 246.
- [3] Y. Nambu and G. Jona-Lasinio, Phys. Rev. **122** (1961) 345.
- [4] J. B. Kogut and L. Susskind, Phys. Rev. D **11**, 395 (1975).
- [5] Y. Nambu, Phys. Rev. D **10**, 4262 (1974).
- [6] S. Mandelstam, Phys. Rept. **23**, 245 (1976).
- [7] G. 't Hooft, Nucl. Phys. B **190**, 455 (1981).
- [8] Color Confinement and Hadrons in Quantum Chromo-dynamics edited by H. Suganuma, N. Ishii, M. Oka, H. Enyo, T. Hatsuda, T. Kunihiro, and K. Yazaki (World Scientific, 2004)

- [9] T. Banks and A. Casher, Nucl. Phys. B **169**, 103 (1980).
- [10] A. M. Garcia-Garcia and J. C. Osborn, Phys. Rev. D **75**, 034503 (2007) [arXiv:hep-lat/0611019].
- [11] A. Gocksch and M. Ogilvie, Phys. Rev. D **31**, 877 (1985).
- [12] S. Digal, E. Laermann and H. Satz, Eur. Phys. J. C **18**, 583 (2001) [arXiv:hep-ph/0007175].
- [13] K. Fukushima, Phys. Rev. D **68**, 045004 (2003) [arXiv:hep-ph/0303225].
- [14] T. A. DeGrand and D. Toussaint, Phys. Rev. D **22**, 2478 (1980).
- [15] J. S. Barber, R. E. Shrock and R. Schrader, Phys. Lett. B **152**, 221 (1985).
- [16] V. Grosch, K. Jansen, J. Jersak, C. B. Lang, T. Neuhaus and C. Rebbi, Phys. Lett. B **162**, 171 (1985).
- [17] J. S. Barber and R. E. Shrock, Nucl. Phys. B **257** (1985) 515.
- [18] J. B. Kogut and E. Dagotto, Phys. Rev. Lett. **59**, 617 (1987).
- [19] V. Azcoiti, Phys. Lett. B **194** (1987) 438.
- [20] E. Dagotto and J. B. Kogut, Nucl. Phys. B **295**, 123 (1988).
- [21] V. Azcoiti, G. di Carlo and A. F. Grillo, Phys. Lett. B **238**, 355 (1990).
- [22] M. Salmhofer and E. Seiler, Commun. Math. Phys. **139**, 395 (1991) [Erratum-ibid. **146**, 637 (1992)].
- [23] S. Hashimoto, M. Kikugawa and T. Muta, Phys. Lett. B **254**, 449 (1991).
- [24] H. Gausterer and C. B. Lang, Phys. Lett. B **263**, 476 (1991).
- [25] V. Azcoiti, G. Di Carlo and A. F. Grillo, Phys. Lett. B **268**, 101 (1991).
- [26] V. Azcoiti, I. M. Barbour, R. Burioni, G. Di Carlo, A. F. Grillo and G. Salina, Phys. Rev. D **51**, 5199 (1995).
- [27] M. Baig, H. Fort and J. B. Kogut, Phys. Rev. D **50**, 5920 (1994) [arXiv:hep-lat/9406004].
- [28] H. Shiba and T. Suzuki, Phys. Lett. B **343**, 315 (1995) [arXiv:hep-lat/9406010].
- [29] T. Bielefeld, S. Hands, J. D. Stack and R. J. Wensley, Phys. Lett. B **416**, 150 (1998) [arXiv:hep-lat/9709047].
- [30] J. Cox, W. Franzki, J. Jersak, C. B. Lang and T. Neuhaus, Nucl. Phys. B **532**, 315 (1998) [arXiv:hep-lat/9705043].
- [31] B. A. Berg, H. Markum and R. Pullirsch, Phys. Rev. D **59**, 097504 (1999) [arXiv:hep-lat/9812010].
- [32] B. A. Berg, U. M. Heller, H. Markum, R. Pullirsch and W. Sakuler, Phys. Lett. B **514**, 97 (2001) [arXiv:hep-lat/0103022].
- [33] G. Arnold, B. Bunk, T. Lippert and K. Schilling, Nucl. Phys. Proc. Suppl. **119**, 864 (2003) [arXiv:hep-lat/0210010].

- [34] T. Drescher and C. B. Lang, JHEP **0502** (2005) 058 [arXiv:hep-lat/0411012].
- [35] M. Vettorazzo and P. de Forcrand, Phys. Lett. B **604**, 82 (2004) [arXiv:hep-lat/0409135].
- [36] M. Panero, JHEP **0505**, 066 (2005) [arXiv:hep-lat/0503024].
- [37] A. Hart and M. Teper, Phys. Rev. D **58**, 014504 (1998) [arXiv:hep-lat/9712003].
- [38] H. Neuberger, Phys. Lett. B **417**, 141 (1998) [arXiv:hep-lat/9707022].
- [39] H. Neuberger, Phys. Lett. B **427**, 353 (1998) [arXiv:hep-lat/9801031].
- [40] M. Luscher, Phys. Lett. B **428**, 342 (1998) [arXiv:hep-lat/9802011].
- [41] P. H. Ginsparg and K. G. Wilson, Phys. Rev. D **25**, 2649 (1982).
- [42] L. Giusti, C. Hoelbling, M. Luscher and H. Wittig, Comput. Phys. Commun. **153**, 31 (2003) [arXiv:hep-lat/0212012].
- [43] P. Hernandez, K. Jansen and M. Luscher, Nucl. Phys. B **552**, 363 (1999) [arXiv:hep-lat/9808010].
- [44] R. B. Morgan and M. Zeng, Linear Algebra and its Applications **415**, 96 (2006)
- [45] F. Farchioni, arXiv:hep-lat/9902029.
- [46] H. Reinhardt, O. Schroeder, T. Tok and V. C. Zhukovsky, Phys. Rev. D **66**, 085004 (2002) [arXiv:hep-th/0203012].
- [47] R. Pullirsch, K. Rabitsch, T. Wettig and H. Markum, Phys. Lett. B **427**, 119 (1998) [arXiv:hep-ph/9803285].
- [48] H. Markum, W. Plessas, R. Pullirsch, B. Sengl and R. F. Wagenbrunn, arXiv:hep-lat/0505011.
- [49] P. W. Anderson, Phys. Rev. **109** (1958) 1492.
- [50] M. V. Berry and M. Tabor, J. Phys. A **10** (1977) 371.
- [51] O. Bohigas, M. J. Giannoni and C. Schmit, Phys. Rev. Lett. **52**, 1 (1984).
- [52] T. S. Biro, C. Gong, B. Muller and A. Trayanov, Int. J. Mod. Phys. C **5**, 113 (1994) [arXiv:nucl-th/9306002].
- [53] T. S. Biro, M. Feurstein and H. Markum, Heavy Ion Phys. **7**, 235 (1998) [arXiv:hep-lat/9711002].
- [54] L. Salasnich, Mod. Phys. Lett. A **12**, 1473 (1997) [arXiv:quant-ph/9706025].
- [55] C. Mukku, M. S. Sriram, J. Segar, B. A. Bambah and S. Lakshmibala, J. Phys. A **30**, 3003 (1997) [arXiv:hep-th/9610071].
- [56] C. Gatttringer, E. M. Ilgenfritz and S. Solbrig, arXiv:hep-lat/0601015.

